Mon. Not. R. Astron. Soc. **000**, 1–7 (2009) Printed 31 August 2009 (MN LATEX style file v2.2)

High Resolution 3D Relativistic MHD Simulations of Jets

A. Mignone[1⋆], P. Rossi[2], G. Bodo[2], A. Ferrari[1] and S. Massaglia[1]
[1] *Dipartimento di Fisica Generale dell Universitá di Torino, Italy*
[2] *INAF Osservatorio Astronomico di Torino, Italy*

arXiv:0908.4523v1 [astro-ph.CO] 31 Aug 2009

31 August 2009

ABSTRACT

Relativistic magnetized jets are key elements in Active Galactic Nuclei and in other astrophysical environments. Their structure and evolution involves a complex nonlinear physics that can be approached by numerical studies only. Still, owing to a number of challenging computational aspects, only a few numerical investigations have been undertaken so far. In this paper, we present high-resolution three dimensional numerical simulations of relativistic magnetized jets carrying an initially toroidal magnetic field. The presence of a substantial toroidal component of the field is nowadays commonly invoked and held responsible for the process of jet acceleration and collimation. We find that the typical nose cone structures, commonly observed in axisymmetric two-dimensional simulations, are not produced in the 3D case. Rather, the toroidal field gives rise to strong current driven kink instabilities leading to jet wiggling. However, it appears to be able to maintain an highly relativistic spine along its full length. By comparing low and high resolution simulations, we emphasize the impact of resolution on the jet dynamical properties.

Key words: galaxies: jets – magnetohydrodynamics (MHD) – instabilities – relativity

1 INTRODUCTION

Understanding the dynamics of relativistic jets is an essential step for the comprehension and interpretation of many phenomenological properties of Active Galactic Nuclei. Magnetic fields appear to be an essential ingredient in their structure: observations of highly polarized non-thermal synchrotron radiation evince the presence of partially ordered magnetic fields, e.g., Gabuzda et al (2004); Laing et al (2008); Gabuzda et al (2008). In particular, it is likely that a toroidal component prevail on large scales as the poloidal component decays as $B_p \propto 1/R_j^2$ while the toroidal $B_\phi \propto 1/R_j$, where $1/R_j$ is the jet radius that expands from the inner galactic core to the radio jet lobes. From the theoretical point of view toroidal magnetic fields are the necessary element of the widely accepted magnetically driven mechanisms for jet acceleration and collimation by fields with footpoints attached to a spinning black hole or accretion disc (Lovelace 1976; Blandford 1976; Blandford & Payne 1984; Narayan et al. 2007).

On the other hand cylindrical magnetohydrodynamic (MHD) configurations are subject to many unstable modes, as reflection modes, Kelvin-Helmholtz modes, current carrying modes, etc. In particular configurations in which toroidal magnetic fields dominate are known to be violently unstable to the $m = 1$ kink instability according to the Kruskal-Shafranov criterion (Bateman 1978)

$$\left|\frac{B_\phi}{B_p}\right| > \frac{2\pi R_j}{z}$$

where z is the jet length. Instead astrophysical jets appear to be quite stable and this becomes an unsolved issue, although several proposals have been made, related to the formation of cocoons by the bow shock at the head of the jet (Begelman 1998), (Massaglia et al. 1996) or the jet expansion (Moll et al. 2008; McKinney & Blandford 2009), or wave coupling with MHD modes producing particle acceleration (Benford et al. 1980).

On the other hand, one may wonder whether the main jet constituent is electromagnetic energy in the form of Poynting-dominated beams, rather than mass. However, Sikora et al. (2005) argued that, even though jets could be Poynting-dominated at the origin, observational data suggest that they become kinetically dominated beyond about 1,000 gravitational radii from the central acceleration region, powered by a super-massive black-hole of $\sim 10^{8-10}$ $M_\odot$.

The mechanism by which the toroidal field responsible for the jet acceleration can be dissipated may be related to the above mentioned instabilties. In this respect Giannios & Spruit (2006) (see also Eichler 1993; Begelman 1998) analyzed the role of the kink instability in magnetically driven jets and concluded that the Poynting flux can be rapidly dissipated and the jet becomes kinetically-dominated, again at about 1,000 gravitational radii.

⋆ E-mail: mignone@ph.unito.it (AM)

Recently, McKinney & Blandford (2009) showed that relativistic jets produced in proximity of rapidly spinning black-holes with dipolar magnetic fields expand rapidly and can survive up to large radii without showing appreciable disruption due to the dominant $m = 1$ kink mode. Their simulations were carried out using large-scale global general relativistic simulations in three-dimensional spherical coordinates adopting a modest resolution to capture both the disk and the jet dynamics. Three-dimensional simulations of the jet formation and evolution in the general relativistic MHD domain has been performed as well by Nishikawa et al. (2005) in the case of a Schwarzschild black hole accretion disk system.

It is therefore crucial to study in a more systematic fashion the fate of relativistic magnetized jets in this transition region, examine the model parameter space to find whether the above requirements and predictions can be met. Relativistic jets carrying magnetic fields can be described by the equations of relativistic MHD (RMHD) and only in the last decade considerable efforts have been spent towards obtaining more robust and accurate numerical schemes. This opened the door to noticeable advancements in the field of numerical simulations. A first study of the properties of two-dimensional relativistic magnetized jets has been performed by Komissarov (1999) and subsequently they have been thoroughly analyzed by Leismann et al. (2005); Mignone et al. (2005); Keppens et al. (2008). Mizuno et al. (2007) have, instead, studied the instability of a 3D RMHD cylindrical flow.

In this paper we present the first high-resolution (to our knowledge) numerical simulations of the propagation in three dimensions of a (special) relativistic magnetized jet injected in a uniform un-magnetized external medium. Computations are carried out at both high ($640 \times 1600 \times 640$ cell, with 20 pts/beam radius) and low ($320 \times 800 \times 320$, with 10 pts/beam) resolution. A comparison between the two reveals the importance of high resolution, especially for this class of astrophysical phenomena. We consider jets initially carrying a purely toroidal magnetic field: as previously said, the presence of this component is intimately connected to the jet formation mechanism and it is likely to affect the jet dynamics through the onset of current driven (CD) instabilities. In this respect, it is of great interest to analyse their growth and evolution. Previous non-relativistic three dimensional simulations of Nakamura & Meier (2004) revealed that strongly magnetized supersonic jets develop CD induced distortions and that the kink ($m = 1$) mode grows faster than the other modes. More recently, Moll et al. (2008) have studied the generation and propagation of a nonrelativistic jet with a self-consistent toroidal field component, showing and analysing the development of these instabilities. In the present work we investigate the relativistic case, starting with the limiting case of a purely toroidal field which, at least in the Newtonian case, is known to be the most unstable configuration. Our study extends previous 3D simulations of the propagation of unmagnetized relativistic jets (Rossi et al. 2008) and, in the following, we will often refer to these results for comparison. The effects of different field configurations and physical parameters will be examined in a forthcoming paper.

In the next section we describe our numerical setup, in §3 we outline the simulation results and in §4 we summarize our conclusions.

2 NUMERICAL SETUP

Numerical simulations are carried out by solving the equations of special relativistic MHD (RMHD) in conservation form (Anile 1990):

$$\begin{aligned} \partial_\mu \left(\rho u^\mu\right) &= 0\,, \\ \partial_\mu \Big(w u^\mu u^\nu - b^\mu b^\nu + p\eta^{\mu\nu} \Big) &= 0\,, \\ \partial_\mu \left(u^\mu b^\nu - u^\nu b^\mu\right) &= 0\,, \end{aligned} \tag{1}$$

where ρ is the rest mass density, $u^\mu \equiv \gamma(1, \boldsymbol{v})$ and $b^\mu = (b^0, \boldsymbol{B}/\gamma + b^0\boldsymbol{v})$ are the four-velocity and covariant magnetic field written in terms of the three velocity $\boldsymbol{v}$ and laboratory magnetic field $\boldsymbol{B}$ and $b^0 = \gamma\boldsymbol{v}\cdot\boldsymbol{B}$. A flat metric $\eta^{\mu\nu} = \mathrm{diag}(-1, 1, 1, 1)$ is considered. In the previous equations $w = w_{\rm g} + b^2$ and $p = p_g + b^2/2$ express the total enthalpy and total pressure in terms of their thermal ($w_{\rm g}$ and $p_{\rm g}$) and magnetic contributions ($b^2 = b^\mu b_\mu$), respectively. An additional equation, describing the advection of a passive scalar (or tracer) $f(x, y, z, t)$, is included to discriminate between jet material (where $f = 1$) and the environment (where $f = 0$). We assume a single-specie relativistic perfect fluid (the Synge gas) described by the approximated equation of state proposed by Mignone et al. (2005) and Mignone & McKinney (2007).

The computational domain is initially filled with an unmagnetized medium at rest, with uniform density ρ_a and gas pressure p_a. The jet flows parallel to the y direction through a cylindrical nozzle specified by $r = \sqrt{x^2 + z^2} < 1$ (in units of the jet radius) at the lower boundary. At the nozzle, the beam has constant density ρ_j and longitudinal velocity component (v_y) given in terms of the Lorentz factor γ_j, whereas the magnetic field carries a purely toroidal (i.e. azimuthal) component:

$$B_\phi(r) = \begin{cases} B_m r/a & \text{for} \quad r < a\,, \\ B_m a/r & \text{for} \quad r > a\,, \\ 0 & \text{for} \quad r > 1\,, \end{cases} \tag{2}$$

where $a = 1/2$ is the magnetization radius. The pressure profile follows from the numerical integration of the radial momentum balance equation across the beam:

$$\frac{\partial}{\partial r}\left(p_g + \frac{b^2}{2}\right) = \frac{w u_\phi^2 - b_\phi^2}{r}\,. \tag{3}$$

where a small differential rotation is assumed by setting $u_\phi = \alpha\gamma B_\phi/B_m$ with $\alpha = 0.2$. The pressure profile $p(r)$ is continuous across the jet boundary, i.e., $p_a = p_j(1)$. The integration constant and the field strength B_m are specified through the sonic Mach number $M_s = v_j/c_s(a)$ and Alfvénic Mach number $M_A = v_j/v_A(a)$ (c_s and v_A are the sound and Alfvén velocities) at the magnetization radius. Thus the beam values are entirely specified in terms of the density contrast $\eta = \rho_j/\rho_a$, Lorentz factor γ_j, sonic and Alfvénic Mach numbers. Motivated by the results obtained in Rossi et al. (2008), we choose $\eta = 10^{-4}$, $\gamma_j = 10$, $M_s = 3$ and $M_A = 1.67$, so that the ratio of the average gas and

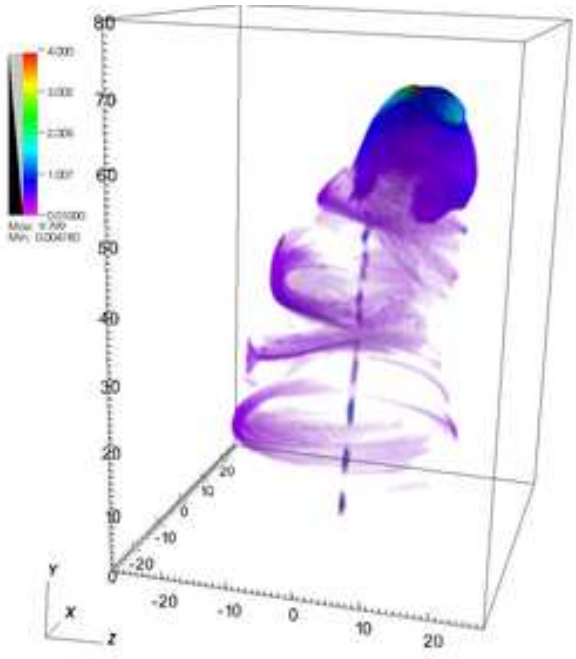

Figure 2. Volume renderings of the thermal pressure distributions at $t = 710$ for the high resolution 3D run.

magnetic pressures is close to one (equipartition). Velocity perturbations are super-imposed as in Rossi et al. (2008). Reflective boundary conditions hold at $y = 0$ outside the inlet region and zero-gradient is assumed through the remaining boundaries.

Simulations are carried out with the PLUTO code for astrophysical gasdynamics (Mignone et al. 2007). The chosen configuration employs a second order Godunov type scheme with the recently developed HLLD Riemann solver (Mignone et al. 2009) and the mixed hyperbolic/parabolic divergence cleaning by Dedner et al. (2002) to control the solenoidal constraint. Our computational box is defined by $x \in [-L/2, L/2]$, $y \in [0, L_y]$ and $z \in [-L/2, L/2]$, ($L = 56$, $L_y = 80$) with a uniform resolution in $|x|, |z| < 10$ and a geometrically stretched grid otherwise. Both low (10 points per beam radius) and high (20 zones) resolution simulations are performed, yielding an overall resolution of $320 \times 800 \times 320$ and $640 \times 1600 \times 640$ computational zones, respectively.

3 RESULTS

In the left panel of Fig. 1 we show the volume renderings of the tracer distribution when the jet has reached the length of ~ 70 beam radii. For the sake of comparison we also show, in the right panel, the rendering of an equivalent 2-D axisymmetric simulation with the same parameters. The picture (in the right panel) clearly indicates the presence of a nose cone structure typical of two-dimensional high Poynting flux jets (Clarke et al. 1986; Lind et al. 1989; Komissarov 1999; Leismann et al. 2005), originating from the amplification at the terminal shock of the toroidal field component which then confines the jet material and prevents it to freely flow in the cocoon. In three dimensions, however, this structure

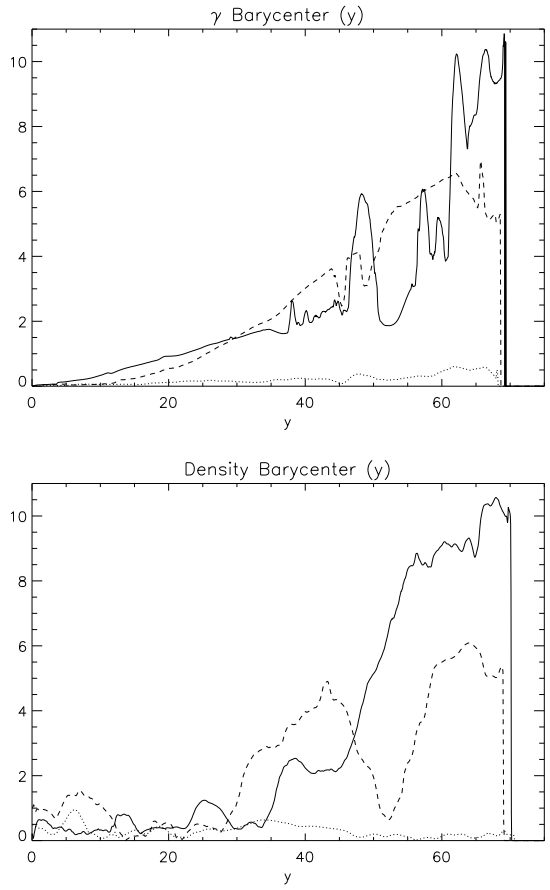

Figure 3. Barycenter Displacements from the longitudinal axis $\bar{r}$ of the Lorentz factor (top) and jet laboratory density (bottom) for the high resolution (solid lines), low resolution (dashed lines) and hydro (dotted lines) cases. The corresponding integration times are $t = 710$, $t = 840$ and $t = 590$, respectively.

becomes unstable and does not form leading to a very different asymmetric morphology. In following the jet propagation, we observe that its trajectory becomes progressively more curved, moving away from the longitudinal y axis. This effect becomes more pronounced at the jet head and can be attributed to the presence of current driven kink instabilities. Moreover, the backflowing material forms a very asymmetric cocoon as a result of the changes in direction of the jet head. In Fig. 2, representing the pressure distribution, it is possible to observe two regions of enhanced pressure in the bow shock. Comparing the tracer and pressure distributions, we can identify these areas as the points where the jet is more strongly deflected. The asymmetric backflow appears to be quite pronounced, reaching relatively high velocities up to $0.9c$.

The displacement of the beam from the longitudinal axis plays a fundamental role in the jet morphology and it is evaluated, at each position along the jet, by the quantity $\bar{r}(y) = \sqrt{\bar{x}^2 + \bar{z}^2}$, where

$$\bar{x}(y) = \frac{\int x Q dx\, dz}{\int Q dx\, dz}, \quad \bar{z}(y) = \frac{\int z Q dx\, dz}{\int Q dx\, dz}. \tag{4}$$

where Q can be any flow quantity. Choosing $Q = \gamma\chi$, where $\chi = 1$ for $\gamma > 1.5$ and $\chi = 0$ otherwise, gives a measure of the

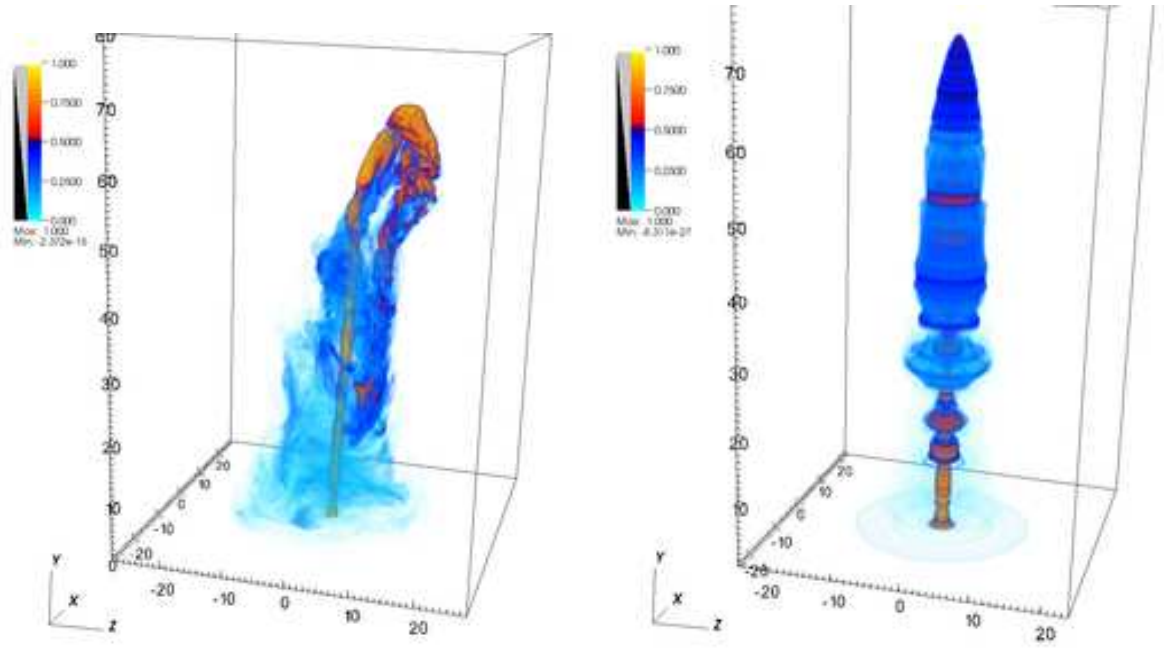

Figure 1. Volume renderings of the passive scalar distributions for the high resolution 3D run (left panel) and 2D axisymmetric case (right) at $t = 710$.

distance of the Lorentz factor centroid from the axis. Likewise, we can quantify the jet density barycenter by choosing $Q = \rho\gamma f$. In Fig. 3 we plot both the Lorentz factor and density centroids as functions of y. Solid, dashed and dotted lines refer, respectively, to the high resolution, low resolution and non magnetized case with the same parameters (Lorentz factor, density ratio and Mach numbers). Simulation times have been chosen so that the jets have reached approximately the same distance, ~ 70 radii. Both the low and high resolution cases show moderate displacements up to ~ 40 jet radii followed by a strong increase soon after. The effect is more pronounced in the high resolution case, eventually reaching maximum values in excess of 10. On the contrary, no significant deviations are seen in the purely hydro case and the beam propagates very close to the initial axis.

Fig. 4 represents the distribution of the jet mass fraction moving at a certain value of $\gamma\beta$ at the end of the simulation when the jet has traveled approximately 70 beam radii. Both low (top panel) and high (bottom panel) resolution cases are shown. We use the four-velocity (instead of the Lorentz factor) to avoid compression of the scale close to $\gamma = 1$, i.e. at low velocities. The legend on the right gives the corresponding value of $\gamma\beta$ for each color. As an illustrative example, one can see that at $y = 15$ the mass fractions moving with $\gamma\beta > 6$, $\gamma\beta \in [5, 6]$,$\gamma\beta \in [4, 5]$,$\gamma\beta \in [3, 4]$ and $\gamma\beta < 3$ are, respectively, 10%, 10%, 20%, 25% and 35%. Focusing on the high velocity part of the distribution, we can observe the presence of material moving at $\gamma \sim 10$ all along the jet (red spots close to the y-axis). The behavior of the low resolution case, shown in the upper panel, is quite different. Jet material moves at $\gamma \sim 10$ only up to $y \sim 20$, with a decrease of the maximum Lorentz factor to a value of about 5.

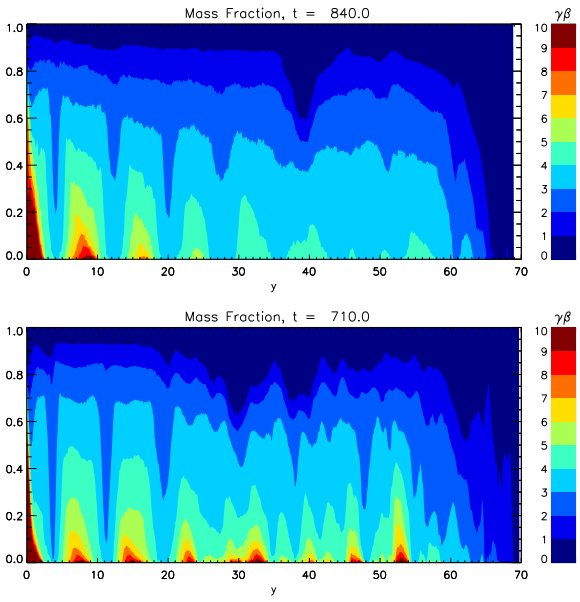

Figure 4. Jet mass fraction for the low resolution (top panel) and high resolution (bottom panel) cases.

The toroidal field seems to protect the jet core from any interaction with the surrounding, thus preventing momentum transfer to the external medium. This behavior is better understood by inspecting the top panel in Fig. 5 where we show the jet cross-section (in the high resolution case) at different positions along the longitudinal axis. For comparison, a similar plot for the unmagnetized case, shown in the bottom panel, reveals that in this case the jet surface is deformed by non-axisymmetric modes of high order

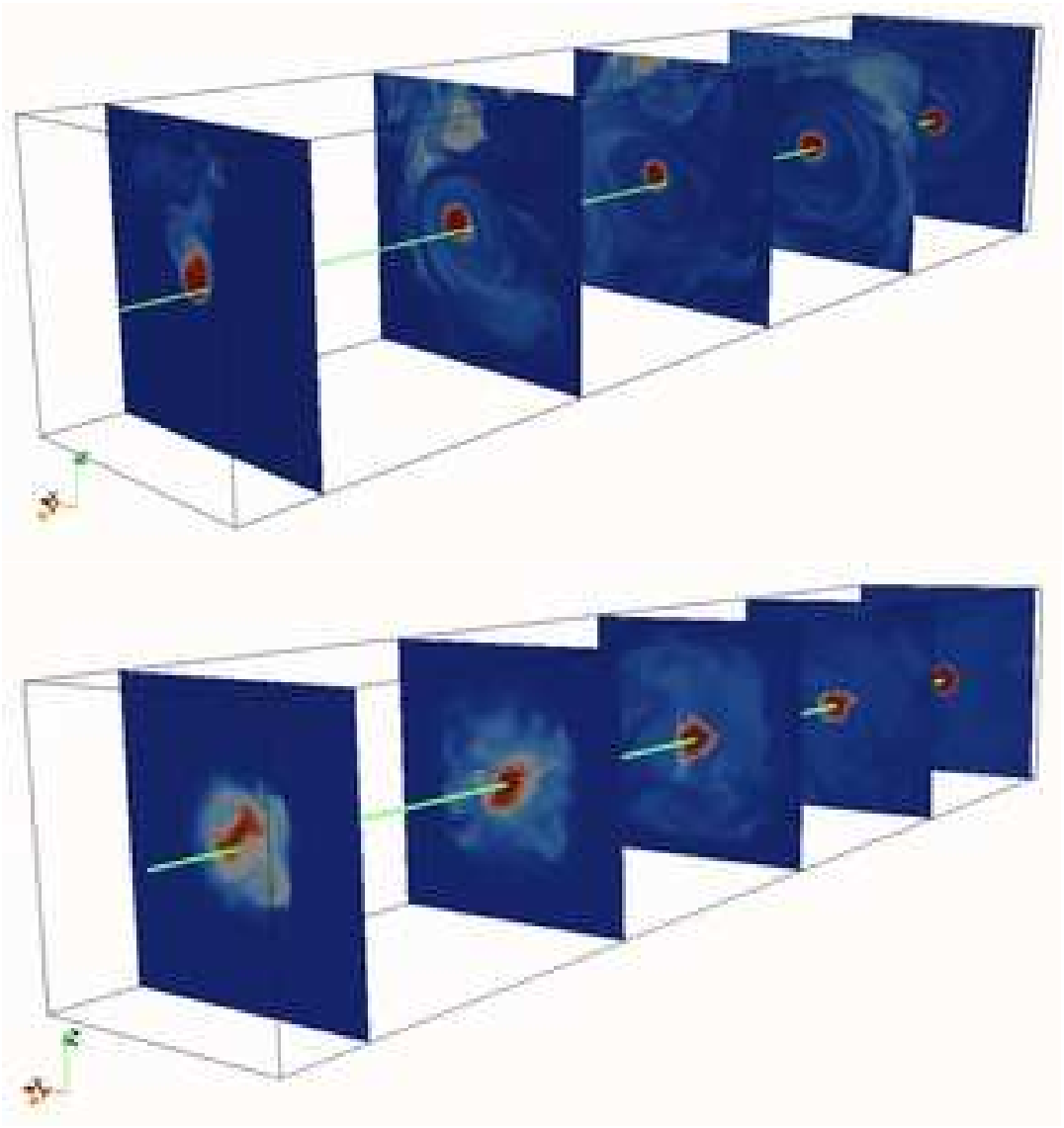

Figure 5. Two dimensional slices at constant y planes for the high resolution magnetized case (top panel) and purely hydrodynamical case (bottom, low resolution). The solid line marks the longitudinal axis $(x, z = 0)$ while the line of sight is such that the jet propagates from the furthest boundary to the closer one.

$(m > 2)$ promoting mixing between jet material and external medium. On the contrary, the high resolution magnetized case shows the presence of low order modes $(m \leqslant 2)$ only, producing oval deformations that cannot induce any mixing. The tension of the toroidal field, in fact, acts as a strong stabilizing factor for high order modes. Our results are thus in agreement with those of Rosen et al. (1999) where the presence of a toroidal field was shown to noticeably lessen the growth and amplitude of small wavelength modes.

From Fig. 4 one notices also the periodic decrease of the maximum Lorentz factor associated with jet pinching and the formation of periodic shocks along the beam, also visible in the left panel of Fig. 2, where it is possible to follow the appearance of periodic compressions all along the jet. The formation of these internal shocks has been observed in all jet simulations and is in general attributed to the interaction of the cocoon with the jet proper and to Kelvin-Helmholtz instabilities. Three-dimensional effects seemed to decrease the importance of these internal shocks. Indeed, in a similar hydro case (Rossi et al. 2008) at the same resolution, we observed their presence only in the first half of the jet. Here, the decreased interaction of the jet core with the ambient favors their formation and, besides, the additional pinching effect of the toroidal field increases the compression factor. At the same time, the presence of the toroidal field has also the effect of reducing the distance between the shocks when compared to the hydro case. We have seen that, in the case that we are examining, the jet core is protected by the toroidal field and maintains its initial Lorentz factor all along its length. However, it is interesting to ask whether an effect of mixing and entrainment can actually take place on the more external jet layers. From Fig. 4 we can observe that the mass fraction of the material with $\gamma\beta < 2$ varies between 20% in the region closer to the jet origin, to about 30% at outer positions, while in the hydro case this fraction reached values of more than 50% (Rossi et al. 2008),

showing a smaller entrainment efficiency in this case. Correspondingly, a larger fraction of the jet material moves at higher values of $\gamma\beta$.

These results show that, in spite of the large deflection induced by the presence of strong toroidal magnetic field, non-axisymmetric $m = 1$ screw modes do not lead to appreciable jet disruption. These findings agree with those reported in McKinney & Blandford (2009) where the $m = 1$ modes are effective only in modeling the jet substructure without affecting the large-scale dynamics. Although our simulation setup is noticeably different, this qualitative agreement supports the general idea that some other intervening mechanism must act so as to suppress the instability growth, (Moll et al. 2008; Narayan et al. 2009).

The simulation we are discussing has been performed at high resolution employing 20 grid points over the beam radius. Numerical resolution effects are known to be important in jet simulations and, for this reason, we have compared the high resolution computation with a lower resolution one, with only 10 points on the jet radius. In the low resolution case, as it is shown in the upper panel of Fig. 4, numerical diffusion effects tend to increase the deposition of momentum from the jet core to the ambient and therefore the jet is not able to maintain its initial Lorentz factor up to the head. In addition, we have also observed that periodic shocks along the jet appear to be substantially weaker and they are not present all along the jet as in the high resolution case. Besides, as discussed above, the jet displacement results larger at high resolution. This comparison shows that the differences due to grid resolution are substantial and demonstrates the importance of performing high resolution simulations for reproducing more accurately the physical behavior. A question that may occur is obviously whether the resolution employed in this work is sufficient, since our results show that we have not yet reached convergence in the basic jet properties (a complete convergence for this problem cannot be reached). We have shown a tendency towards larger displacements of the jet off the axis as the resolution is increased, although this effect is, in any case, localized at the jet's head. Still, we observe a reduction of the momentum transfer from the inner jet to the ambient as the numerical resolution increases. We expect that these well defined trends in the physical characters of the solution should be maintained by a further increase in resolution, that may be feasible in future studies on this subject. The effects described above may therefore change quantitatively, but the qualitative features that we outlined should remain similar to what we obtain.

The results pertaining to the hydrodynamical cases discussed in Rossi et al. (2008) indicated the density ratio η as the main parameter governing the interaction between the beam and the external medium. In order to investigate the role of η for the present magnetized model, we performed a low resolution computation with $\eta = 100$. The results show that, up to the same length, the jet propagates almost undisturbed, without any sign of kink instability nor of mixing with the ambient medium. We think that the most likely explanation for the difference between the two cases at different density ratios (this parameter has no direct effect on the kink instability) should be related to the different advance velocity of the jet head, that is much larger for $\eta = 100$ than for $\eta = 10,000$. In fact, the unstable perturbations are advected by the jet as they grow. In the case with $\eta = 10,000$ the jet head advances at a velocity that is much lower than the jet velocity and, therefore, the unstable perturbations accumulate at the jet head and have enough time for their growth and can give origin to the jet deformation. In the lower ratio case, instead, the jet head advances at a much higher velocity and the kink instability does not have enough time to grow. In this case its effect should be visible only on a larger scale.

4 CONCLUSIONS

We have presented the first results of a three-dimensional high-resolution numerical study of the propagation of relativistic magnetized jets injected into a uniform medium using the PLUTO code. At the highest resolution, the computations employed 20 points on the jet radius for an overall resolution of $640 \times 1600 \times 640$ zones covering a Cartesian domain of $56 \times 80 \times 56$, in units of the beam radius.

From the variety of possible magnetic field configurations, we decided to start our study by considering jets initially carrying a purely toroidal magnetic field. Indeed, the most accepted jet formation mechanisms predict that this field component has to be present and this strengthen the necessity of understanding its key role on the jet dynamics. The presence of a toroidal component of the field is known to drive current-driven kink instabilities which in our case are responsible for jet wiggling and beam deflection off the main longitudinal axis (Narayan et al. 2009). The deviations tend to become more prominent towards the final parts of the jet, where we measured off-axis displacements in excess of 10 radii over a length of 70 radii. The wandering of the jet head, induced by kink instability effects, may create multiple sites where the jet impacts on the external medium forming strong shocks. This behavior may originate the multiple hot spots that are observed in several radiogalaxies (see e.g. Leahy et al. 1997; Hardcastle et al. 2007). The asymmetry of the backflow is another feature that replicates the observational appearance of several objects.

An additional effect of the toroidal field component seems that of shielding the inner jet core from any interaction with the surroundings and therefore from a loss of momentum. Furthermore, we have observed that the jet remains highly relativistic all along its length. Quasi periodic shocks, formed by the combination of several effects like the interaction with the cocoon and the toroidal field pinching, can be observed all along the jet extension. A spine *plus* sheath layer structure with shocks supports the idea that jets at sub-kpc scale can originate correlated variability at radio frequencies and in X and gamma rays (see for instance recent observations by the AGILE and FERMI missions and the TeV ground arrays Donnarumma et al. (2009); Acciari et al. (2009)). The very high frequency emission would originate in the slower sheath layer by inverse Compton boosting of the optical and X photons produced in the relativistic spine. The X ray emission would be synchrotron emission not self-absorbed and would have variability strictly connected to the gamma ray emission. The radio emission would come from synchrotron emission in an outer region of the jet sheath (Tavecchio & Ghisellini 2008).

Recently Moll et al. (2008) have performed 3D simula-

tions of a Newtonian magnetized jet with a toroidal component and have shown the development of kink instabilities that produce helical jet deformations. In their setup the jet is generated by maintaining a rotation profile in the boundary zones and a spherical grid, with a non uniform spacing in the radial direction, is used to describe the jet propagation.

The comparison between low and high resolutions cases shows significant differences in the formation of shocks along the beam. In the high resolution simulations, shocks appear to be stronger, closer and in a larger number. In addition, the jet is able to keep a highly relativistic core for a longer distance.

The results presented here represent only a first step in the analysis of the behavior of relativistic magnetized jets. We have shown that three dimensional and high resolution effects are important factors in this investigation. In a forthcoming paper we intend to explore the influence of different (e.g. poloidal or helical) field configurations.

ACKNOWLEDGMENTS

The numerical calculations were performed at CINECA in Bologna, Italy, thanks to INAF.

REFERENCES

Acciari, V.A., Aliu, E., Arlen, T., et al. 2009, Science, 325, 444
Anile, A. M. 1990, Relativistic Fluids and Magneto-fluids, by A. M. Anile, pp. 348. ISBN 0521304067. Cambridge, UK: Cambridge University Press, February 1990.,
Bateman, G. 1978, *MHD Instabilities* (Cambridge, MA: MIT Press)
Begelman, M. C. 1998, ApJ, 493, 291
Benford, G., Ferrari, A. & Trussoni, E. 1980, ApJ, 241, 98
Blandford, R.D 1976, MNRAS, 176, 465
Blandford, R. D., & Payne, D. G. 1982, MNRAS, 199, 883
Clarke, D. A., Norman, M. L., & Burns, J. O. 1986, ApJL, 311, L63
Dedner, A., Kemm, F., Kröner, D., Munz, C.-D., Schnitzer, T., & Wesenberg, M. 2002, Journal of Computational Physics, 175, 645
Donnarumma, I., Vittorini, V., Vercellone, S., et al. 2008, ApJL, 691, L13
Eichler, D. 1993, ApJ, 419, 111
Gabuzda, D. C., Murray, É., & Cronin, P. 2004, MNRAS, 351, L89
Gabuzda, D. C., Vitrishchak, V. M., Mahmud, M., & O'Sullivan, S. P. 2008, MNRAS, 384, 1003
Giannios, D., & Spruit, H.C., 2006, A&A, 450, 887
Hardcastle, M. J., Croston, J. H., & Kraft, R. P. 2007, ApJ, 669, 893
Keppens, R.; Meliani, Z.; van der Holst, B.; Casse, F. 2008, Astronomy & Astrophysics. 486, 663
Komissarov, S. 1999, MNRAS, 308, 1069.
Laing, R. A., Bridle, A. H., Parma, P., Feretti, L., Giovannini, G., Murgia, M., & Perley, R. A. 2008, MNRAS, 386, 657
Leahy, J. P., Black, A. R. S., Dennett-Thorpe, J., Hardcastle, M. J., Komissarov, S., Perley, R. A., Riley, J. M., & Scheuer, P. A. G. 1997, MNRAS, 291, 20
Leismann, T., Anton L., Aloy, M. A., Müller, W., Martí, J.M., Miralles, J.A. & Ibanez, J. M. 2005, A&S, 436, 503
Lind, K. R., Payne D. G., Meyer, D. L. & Blandford, R. D. 1989, ApJ, 344, 89
Lovelace, R.V.E. 1976, Nature 262, 649
Massaglia, S., Bodo, G. & Ferrari, A. 1996, Astronomy & Astrophysics. 307, 997
McKinney, J. C., Blandford, R. D., 2009, MNRAS, 394, L126
Mignone, A., Massaglia, S., & Bodo, G. 2005, Space Science Reviews, 121, 21
Mignone, A., Plewa, T., & Bodo, G. 2005, ApJS, 160, 199
Mignone, A., & McKinney, J. C. 2007, MNRAS, 378, 1118
Mignone, A., Bodo, G., Massaglia, S., Matsakos, T., Tesileanu, O., Zanni, C., & Ferrari, A. 2007, ApJS, 170, 228
Mignone, A., Ugliano, M., & Bodo, G. 2009, MNRAS, 393, 1141
Mizuno, Y., Hardee, P., & Nishikawa, K.-I. 2007, ApJ, 662, 835
Moll, R., Spruit, H.C. & Obergaulinger, M. 2008, A&A, 492, 621
Nakamura, M., & Meier, D. L. 2004, ApJ, 617, 123
Narayan, R., McKinney, J.C., & Farmer, A.J. 2007, MNRAS, 375, 548
Narayan, R., Jason, L., Tchekhovskoy, A. 2009, ApJ, 697, 1681
Nishikawa, K.-I., Richardson, G., Koide, S., Shibata, K., Kudoh, T., Hardee, P., & Fishman, G. J. 2005, ApJ, 625, 60
Rosen, A., Hardee, P. E., Clarke, D. A., & Johnson, A. 1999, ApJ, 510, 136
Rossi, P., Mignone, A., Bodo, G., Massaglia, S., & Ferrari, A. 2008, A&A, 488, 795.
Sikora, M., Begelman, M.C., Madejski, G.M., & Lasota, J.-P., 2005 ApJ, 625, 72
Tavecchio, F. & Ghisellini, G. 2008, MNRAS, 385, L98